UC Berkeley
UC Berkeley Previously Published Works

Title

3D microfluidic gradient generator for combination antimicrobial susceptibility testing

Permalink

https://escholarship.org/uc/item/6ht2c2s0

Journal

Microsystems & Nanoengineering, 6(1)

ISSN

2096-1030

Authors

Sweet, Eric
Yang, Brenda
Chen, Joshua
et al.

Publication Date

2020

DOI

10.1038/s41378-020-00200-7

Peer reviewed

ARTICLE

Open Access

3D microfluidic gradient generator for combination antimicrobial susceptibility testing

Eric Sweet [1,2], Brenda Yang[2,3], Joshua Chen[2,3], Reed Vickerman[1,2,4], Yujui Lin[2], Alison Long[2,3], Eric Jacobs [2,3], Tinglin Wu[2,3], Camille Mercier[2,3], Ryan Jew[1,2,3], Yash Attal[2,3], Siyang Liu[1,2], Andrew Chang[2] and Liwei Lin[1,2]

Abstract

Microfluidic concentration gradient generators (μ-CGGs) have been utilized to identify optimal drug compositions through antimicrobial susceptibility testing (AST) for the treatment of antimicrobial-resistant (AMR) infections. Conventional μ-CGGs fabricated via photolithography-based micromachining processes, however, are fundamentally limited to two-dimensional fluidic routing, such that only two distinct antimicrobial drugs can be tested at once. This work addresses this limitation by employing Multijet-3D-printed microchannel networks capable of fluidic routing in three dimensions to generate symmetric multidrug concentration gradients. The three-fluid gradient generation characteristics of the fabricated 3D μ-CGG prototype were quantified through both theoretical simulations and experimental validations. Furthermore, the antimicrobial effects of three highly clinically relevant antibiotic drugs, tetracycline, ciprofloxacin, and amikacin, were evaluated via experimental single-antibiotic minimum inhibitory concentration (MIC) and pairwise and three-way antibiotic combination drug screening (CDS) studies against model antibiotic-resistant *Escherichia coli* bacteria. As such, this 3D μ-CGG platform has great potential to enable expedited combination AST screening for various biomedical and diagnostic applications.

Introduction

Treatment of antimicrobial-resistant (AMR) infections places a significant economic burden on the worldwide economy, upwards of $35 billion per year in the United States alone, and is projected to be the cause of over 10 million deaths per year by year 2050[1–3]. In the context of antibiotic resistance, for instance, more than 18 distinct bacteria, including pathogenic *Escherichia coli* (*E. coli*), *Listeria monocytogenes* (*L. monocytogenes*), and *Staphylococcus aureus* (*S. aureus*), have developed biological resistance to one or more of the world's essential first-line-of-defense antibiotic agents[4,5]. The susceptibility of AMR organisms to antimicrobial compounds is assessed in clinical and biomedical research settings through antimicrobial susceptibility testing (AST) methods, predominantly minimum inhibitory testing (MIC) and combination drug screening (CDS), which are particularly useful in the fight against antibiotic-resistant infections, such as urinary tract infections (UTIs)[6]. Conventional MIC testing[7] (Supplementary Materials Fig. S1a) involves overnight incubation of a patient-collected bacterial sample in the presence of growth media and dilute antibiotic solutions[8] to determine the lowest dose of a single antibiotic required to inhibit the proliferation of bacteria and increase bacterial colony density, which is known as the MIC value[9,10].

The MIC value therefore represents the lowest recommended antibiotic dose effective in treating a particular infection without encouraging further antibiotic resistance[11–13]. Furthermore, the only effective treatment against certain AMR infections is the use of combinations of multiple antimicrobial agents[14–17]. Conventional antibiotic CDS (Supplementary Materials Fig. S1b) is performed in a similar manner to MIC testing yet involves

Correspondence: Eric Sweet (ericsweet@berkeley.edu) or Liwei Lin (lwlin@me.berkeley.edu)
[1]Department of Mechanical Engineering, University of California, Berkeley, CA 94720, USA
[2]Berkeley Sensor and Actuator Center, Berkeley, CA 94720, USA
Full list of author information is available at the end of the article

bacterial incubation in the presence of solutions containing specific ratios of different antibiotic compounds[8,18] to ascertain the combined effects of the antibiotics, whereby certain *synergistic* antibiotic combinations are more effective at inhibiting bacterial proliferation than either of the two antibiotics on their own, while different combinations are either antagonistic, less effective, or additive, exhibiting neither combined effect[19,20].

Conventional AST techniques, while well-established, generally require multiple independent manual labor-intensive fluidic handling procedures, involving a minimum of ~16–24 h for sample enrichment and dilution, followed by ~24–72 h for complete AST analysis[8,21]. As a result, the duration from sample collection to delivery of definitive AST results in clinical settings can take anywhere from 2 days to 1 week[10]. A standard clinical procedure while a clinician awaits AST evaluation, therefore, is to prescribe a large dose of a broad-spectrum antibiotic to stop the infection from worsening, which often contributes to the emergence and propagation of AMR in the first place[22−24]. Moreover, while MIC values[9,11] and CDS results[16,20,25] for specific antibiotics and bacterial strains can be found in the literature, antibiotic sensitivity can evolve over the lifetime of a bacterial colony[26]; therefore, frequent MIC and CDS testing is recommended in clinical settings[10,27,28], posing a considerable limitation on AST throughput and overall cost, especially for screening more than two antibiotics at one time[29,30].

Various microfluidic-based AST platforms[23,31] have demonstrated miniaturized and multiplexed fluid handling[32,33] to increase the throughput of AST analysis[29,34,35] and decrease the mortality rate and healthcare costs[36,37] associated with treating clinical AMR-related infections[38,39], for novel drug development[40,41], and for point-of-care clinical dosage recommendations[42−45]. Microfluidic concentration gradient generators (μ-CGGs), the most widely adopted class of microfluidic AST technologies[46] for MIC and CDS studies, employ branching microchannel networks comprised of nodal units to produce diluted concentrations representing a gradient between input species. Discrete concentration gradients, for example, one antibiotic and one buffer solution[47,48], are represented by the independent outputs from the μ-CGG network itself[49], often referred to as discrete μ-drug cocktails[15]. Several discrete μ-CGG devices have been demonstrated for both single-antibiotic MIC testing and CDS studies[29,50] of clinically relevant antibiotics against laboratory-standard bacteria[51], bioengineered strains[52], and cells isolated from biological fluid samples[40,50,53]. The μ-drug cocktail solutions are either used to perform on-chip bacteria culture[54] or are collected as discrete approximately microliter-volume antibiotic solutions for use in off-chip bacteriological experiments[39]. As a result, a

typical duration for rapid AST analysis is on the order of ~6–8 h[55].

The application of μ-CGG enabled devices toward AST involving more than two antimicrobial compounds, however, is fundamentally limited. Traditional MEMS-based microfluidic fabrication approaches are monolithic in nature; as a result, conventional microchannels have inherently two-dimensional geometric complexity and are therefore capable of fluidic routing in essentially only two dimensions[56]. Symmetric fluidic gradients, those capturing all possible combinations of the inputs, are limited to only two distinct fluidic species at a given time (Fig. 1a). Previous μ-CGGs have demonstrated handling of more than two-input fluids; however, such gradients do not produce any combinations of nonadjacent fluidic species and are nonsymmetric (Fig. 1b). Alternative manufacturing approaches, including tedious and error-prone manual alignment and bonding of PDMS layers, have been demonstrated toward generating quasi-3D microfluidic structures; however, numerous limitations of such processes limit the 3D geometric complexity and practical functionality of such CGG designs[57,58].

Given the ever-advancing capabilities, cost reduction and widespread commercial availability of high-resolution ($\leq 100\,\mu$m) 3D-printing technology and additive manufacturing have garnered significant interest recently toward various microfluidic applications[59]; however, previously demonstrated 3D-printed microfluidic devices have fairly limited applicability towards AST applications, and, in particular, none have demonstrated the generation of discrete gradients of more than two antibiotics for AST[60−62]. Since conventional μ-CGG devices are therefore limited to producing μ-drug cocktails that capture the greatest range of possible combinations of only two antibiotics simultaneously, μ-CGG-enabled CDS of three or more antibiotics demonstrates significantly lower throughput and is fundamentally limited[29,63].

This paper reports the design and development of a truly 3D μ-CGG prototype employing a unique 3D microchannel network that is only possible to fabricate using an additive manufacturing-based approach. The only way to accomplish a symmetric gradient of three or more fluids is to perform fluidic routing in truly three dimensions (Fig. 1c). A tetrahedrally arranged network of nodal microchannel units, geometrically symmetric in 3D space and capable of generating three inherently symmetric fluid gradients, was modeled and fabricated. The concentration gradient generation characteristics of the 3D μ-CGG were first theoretically simulated and used to optimize the design through the use of different integrated 3D microfluidic mixing (μ-mixer) structures to best elucidate the analytically predicted behavior; then, the performance of the fabricated prototype was experimentally validated through fluorescence imaging. Finally,
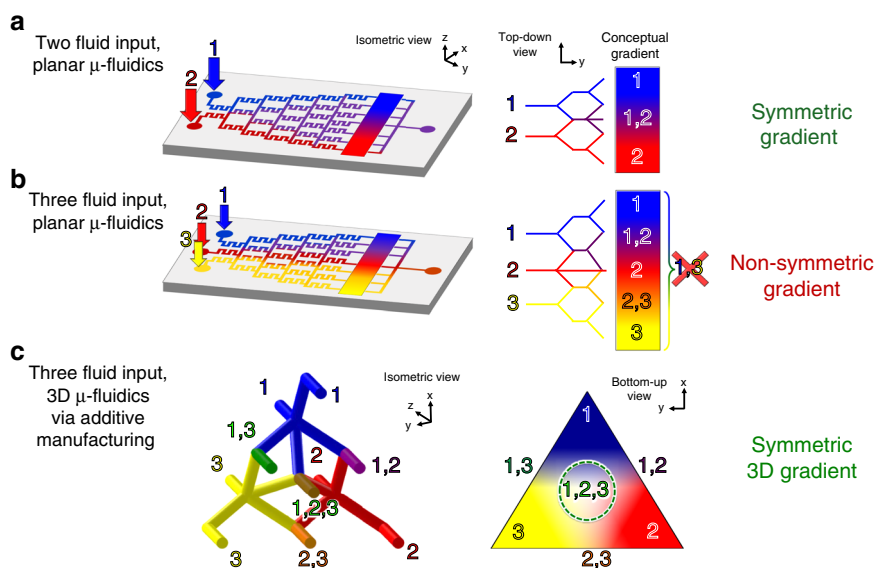
Fig. 1 Conceptual microfluidic concentration gradient generators (µ-CGGs). a Conventional two-input planar devices (e.g., PDMS-based systems fabricated via soft lithography) generate symmetric gradients between both fluids, capturing all possible combinations of both species. **b** Limited to 2D fluidic processing due to the two-dimensionality of monolithic microchannel networks; such devices are unable to generate symmetric fluidic gradients between three or more inputs (i.e., no combinations of fluid inputs 1 and 3 are produced). **c** Only a truly 3D microchannel network capable of 3D fluidic routing, impossible to achieve using planar microfluidic fabrication methods, can generate symmetric 3D gradients of three or more input fluids (i.e., inputs 1 and 2, 2 and 3, 1 and 3, and 1, 2, and 3)

antibiotic gradients collected from the device were used to demonstrate its proof-of-concept utility as an AST tool for MIC testing and pairwise and three-antibiotic CDS bacteriological experiments for three clinically relevant antibiotics against antibiotic-resistant *E. coli* bacteria.

Results

3D µ-CGG design

The 3D µ-CGG microchannel network (Fig. 2a) features three fluidic input channels and 13 discrete output channels. The manufacturable design, consisting of microchannels as hollow structures in a solid body, is shown in Fig. 2b. Briefly, the network is comprised of a truly symmetric 3D arrangement of tetrahedrally arranged nodal combination–mixing–splitting units (Fig. 2b, c, insets). Fluids enter each nodal unit through a vertical channel, here shown with a channel-penetrating 3D-rifled microstructure (3D rifled µ-mixer) integrated into the sidewall, into a hollow spherical bulb (Supplementary Materials Sec. S1.3); then, the fluids flow symmetrically through independent outlets to the next nodal units. The network features three distinct layers of nodal units accomplishing truly symmetric fluidic routing in all three dimensions, generating equivalent proportions of the fluidic inputs to device inlets 1 & 2, 2 & 3, 1 & 3 and, most critically, 1, 2, & 3 at discrete outlets, which is impossible to achieve with planar fluidic routing. Comprehensive analyses of pressure-driven CGG networks using electric

circuit analogies were published in seminal reviews in refs [49,64]. Mathematical approaches traditionally used in the design of conventional 2D CGG's[48,65] were extended in this work to develop a nodal analytical methodology that was used to analytically calculate the expected output flow rates (Q_i) and concentration of each input fluidic species (C_i) at each nodal unit (Fig. 2b, inset) and device outlet (Supplementary Material Sec. S1.5). The fabricated and post processed (Fig. 2c) 3D µ-CGG prototype is shown in Fig. 2d, along with the experimental setups used to collect (Fig. 2e), incubate, and analyze (Fig. 2f) the output solutions. Further analysis of the resolution of the fabricated internal microstructures is presented in Supplementary Materials Sec. S4.

Simulated concentration gradient generation performance

One important assumption made during the analytical calculations of Q_i and C_i at each device outlet is that all fluids are completely mixed when they split off from a given nodal microchannel unit. The accuracy of the Q_i and C_i parameters of each fluidic output of the fabricated 3D µ-CGG prototype to the analytically calculated values is therefore highly dependent on the microfluidic mixing efficiency achieved by each nodal unit. To enhance the mixing quality inside each nodal unit, the effect of integrating intrachannel 3D µ-mixer structures into the sidewall of each vertical microchannel between the upper bulbs (where fluids combine) and the lower bulbs (where
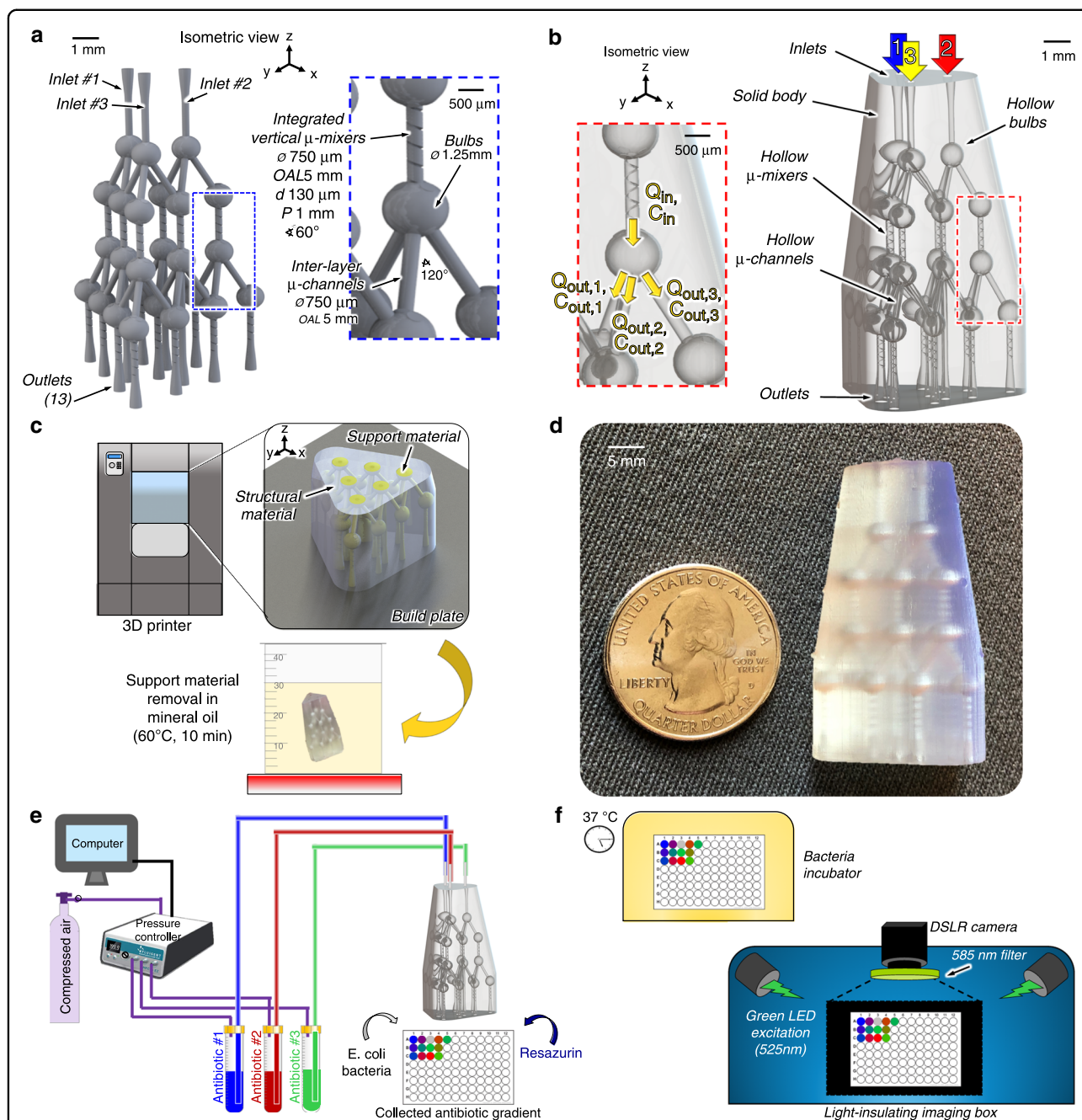
Fig. 2 Developed 3D μ-CGG prototype and experimental setup. a 3D microchannel network design, dimensions, and an indication of labeling convention of device inlets 1, 2, and 3; positive solids model of all hollow structures comprising the truly symmetric 3D arrangement of nodal tetrahedral units (blue inset). **b** Reverse solids model, representing the manufacturable 3D microfluidic design comprising a single solid body with imbedded hollow microchannel structures; (red inset) flow rates (Q_{in}, Q_{out}) and input species concentrations (C_{in}, C_{out}) into and out of each nodal unit; these variables are used in all analytical device output calculations; fluid inputs indicated by colored arrows. **c** Concept of (top) 3D-printing fabrication and (bottom) postprocessing method to remove internal support material. **d** Fabrication results, actual 3D μ-CGG prototype after postprocessing; hollow interior structures are visible through the semitranslucent structural material, with US quarter for scale. Conceptual illustrations of the experimental setups to (**e**) collect the antibiotic gradient outputs from the fabricated 3D μ-CGG device and to (**f**) perform biological incubation and fluorescence imaging to quantify bacterial proliferation

Fig. 3 Theoretical performance of various 3D *μ*-CGG designs from COMSOL CFD simulations. a Analytical calculations for all 3D microchannel network designs are independent of the fluidic flow rate and outlet-numbering convention shown on the right and bottom. Theoretical results for (**b**) a design incorporating smooth-walled vertical channels, **c** a design incorporating vertical channels with repeating hollow spherical sidewall indentations, and **d** a design incorporating vertical channels with imbedded 3D rifling in the sidewalls. Plots (left) of normalized concentration of a single-input fluidic species from one of three device inlets at all 13 device outlets versus input fluid flow rate from 0 to 4000 μL/min, highest percent differences between analytical and simulated results are indicated in red, and the results at 1000 μL/min are also tabulated in Table 1; visualizations (right) of the concentration distribution on all surfaces of the positive solids model of the 3D microchannel network. The 3D rifled *μ*-mixer-integrated design in (**d**) exhibits the lowest error (within 10%) at all outlets and is the design chosen for prototyping, experimental characterization, and demonstration

the fluids split off from) was investigated by studying three different 3D *μ*-CGG designs incorporating (i) smooth-walled vertical channels, serving as a reference, and imbedded (ii) 3D bulbous and (iii) 3D rifled microstructures, both based on a previously demonstrated 3D-printed *μ*-mixer[66] to induce chaotic advective fluid motions for enhanced mixing efficiency[67]. The analytically calculated normalized concentrations (N_c) of a single-input fluidic species (C_1) at each outlet of a conceptual device (Fig. 3a) were independent of the input flow rate into the device. The theoretically predicted N_c values from the COMSOL simulation results for all 3D *μ*-CGG models over a range of symmetric input fluids flow rates from 0 to 4000 μL/min (Fig. 3b–d) become independent of input flow rate for all devices around ~1000 μL/min; therefore only the N_c values at ~1000 μL/min were selected for comparison between devices. In addition, all analytical and theoretical results, and the percent errors between the two, are tabulated in Table 1.

The reference *μ*-CGG design (Fig. 3b) exhibited the highest percent errors in theoretical N_c at device outlets 2 & 3 and outlets 6 & 8, with averages of ~24% and ~57% error, respectively, due to the inefficient microfluidic mixing inside the smooth-walled vertical microchannels. Furthermore, the 3D bulbous *μ*-mixer-integrated *μ*-CGG design (Fig. 3c) exhibited a comparable degree of inaccuracy at outlets 2 & 3 and outlets 6 & 8, with averages of ~26% and ~60%, respectively, which was likely still the result of incomplete fluidic mixing inside these particular 3D microstructure designs. The 3D rifled *μ*-mixer-integrated *μ*-CGG design (Fig. 3d), on the other hand, demonstrated the most accurate results, as the N_c values at all outlets are within 10% of the analytically calculated values. A conventionally accepted metric for the acceptable error of CGG output concentrations for AST applications is a maximum of 10%[39,49]. From this study, the 3D-rifled *μ*-mixer-integrated *μ*-CGG model was deemed capable of generating accurate (≤10% error) output concentrations representing practically useful proportions of each input fluidic species, i.e., ~1, ~7/10, 5/10, ~3/10, and ~0, in addition to an output capturing a nearly equivalent proportion of all three inputs fluidic

Table 1 Theoretical results from COMSOL CDF simulations, the normalized concentration of a single-input fluidic species from one of three device inlets at all 13 device outlets (row 1) at an input flow rate of 1000 µL/min

Outlet #	1	2	3	4	5	6	7	8	9	10	11	12	13
Analytical	1.00	0.70	0.70	0.50	0.50	0.30	0.33	0.30	0.0	0.0	0.0	0.0	0.0
Rifled μ-mixer	1.00	0.70	0.70	0.50	0.50	0.30	0.33	0.30	0.0	0.0	0.0	0.0	0.0
% error	0%	1.4%	2.9%	0%	2.0%	6.7%	6.7%	3.0%	0%	0%	0%	0%	0%
Bulbous μ-mixer	1.00	0.86	0.90	0.50	0.50	0.09	0.32	0.15	0.0	0.0	0.0	0.0	0.0
% error	0%	22.8%	28.6%	0%	0%	70.9%	3.0%	50.0%	0%	0%	0%	0%	0%
Control channel	1.00	0.87	0.87	0.50	0.50	0.13	0.34	0.13	0.0	0.0	0.0	0.0	0.0
% error	0%	24.3%	24.3%	0%	0%	56.7%	6.7%	56.7%	0%	0%	0%	0%	0%

Row 2: analytical calculations and theoretical results (top), with percent error from analytical values (bottom), for the (row 3) 3D rifled μ-mixer, (row 4) 3D bulbous μ-mixer and (row 5) smooth-walled vertical channel integrated 3D μ-CGG designs. Outlets with percent error higher and lower than 10% are indicated in red and green, respectively.

species, i.e., ~1/3, and was therefore chosen as the most appropriate design for prototype fabrication, experimental characterization, and bacteriological demonstrations.
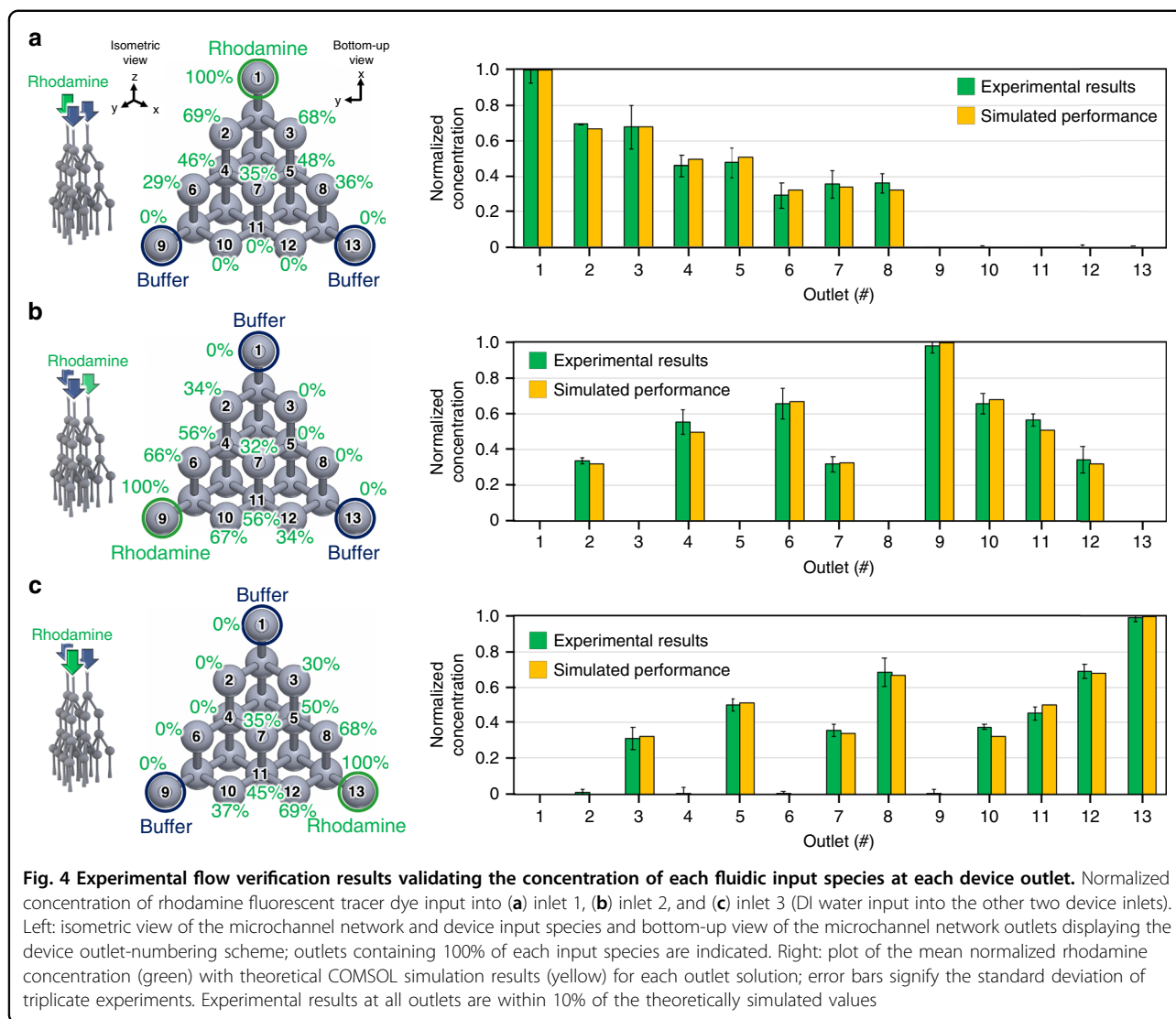
Experimental fluid flow characterization

The experimental characteristics of the fabricated 3D μ-CGG prototype were assessed by using the device to generate a gradient between one rhodamine fluorescent dye solution and two DI water fluidic inputs. Three experiments were performed with the rhodamine solution input into one of the device inlets, i.e., inlet 1, then the process was repeated with the rhodamine solution input into each of the other two inlets, i.e., inlets 2 and 3 (corresponding to the inlet labeling convention shown in Fig. 2a). With the device outputs collected on a 96-well plate, fluorescence imaging was used to measure the fluorescence emission of rhodamine in each solution in order to ascertain the distribution of the rhodamine solution from the device inlet of interest at every output of the device.

With the rhodamine solution used as the input to inlet 1 (Fig. 4a), the mean experimental rhodamine N_c values of all device output solutions were within 10% of the theoretically predicted values from the COMSOL simulation results, exhibiting an average standard deviation of ~4.8%. Likewise, the distributions of rhodamine solution from inlets 2 (Fig. 4b) and 3 (Fig. 4c) among the device outlets produced N_c values within 10% of the theoretically predicted values as well, exhibiting average standard deviations of ~3.9% and ~3.1%, respectively. For further discussion, see Supplementary Material Sec. S7.3. Finally, the experimental N_c values from each experiment were used to quantify the concentration of each of the three fluidic input species contained in every device output solution, in terms of a percentage of the concentration of each input stock solution as presented in Supplementary Material Fig. S11. Regarding practical utility for three-fluid studies, the prototype demonstrated the ability to simultaneously generate three distinct gradients between only two of the three input fluidic species and produced at the outlets along each side of the bottom of the device (e.g., outlets 1, 3, 5, 8, and 13 capture a gradient between fluidic inputs to inlets 1 and 3 without contamination from that from inlet 2). Furthermore, 100% of each fluidic input was produced at outlets 1, 9, and 13; ~50% each of only two fluidic inputs were produced at outlets 4, 5, and 11; and an approximately equivalent proportion (average of ~34%) of each of the three fluidic inputs was produced from outlet 7.

Bacteriological AST demonstrations

The ability of the developed 3D μ-CGG prototype to serve as a microfluidic platform for AST applications was demonstrated through proof-of-concept bacteriological

Fig. 4 Experimental flow verification results validating the concentration of each fluidic input species at each device outlet. Normalized concentration of rhodamine fluorescent tracer dye input into (**a**) inlet 1, (**b**) inlet 2, and (**c**) inlet 3 (DI water input into the other two device inlets). Left: isometric view of the microchannel network and device input species and bottom-up view of the microchannel network outlets displaying the device outlet-numbering scheme; outlets containing 100% of each input species are indicated. Right: plot of the mean normalized rhodamine concentration (green) with theoretical COMSOL simulation results (yellow) for each outlet solution; error bars signify the standard deviation of triplicate experiments. Experimental results at all outlets are within 10% of the theoretically simulated values
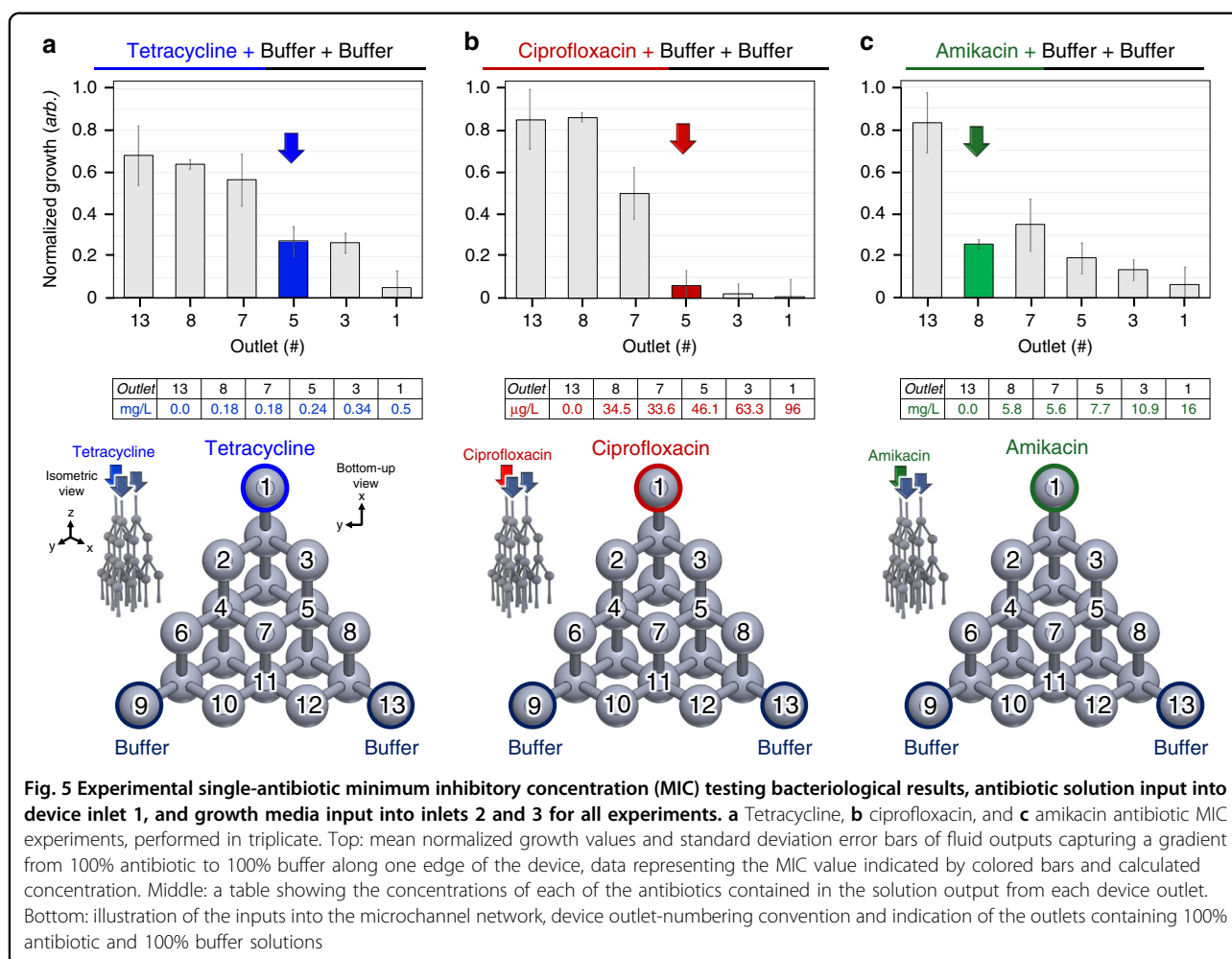
experiments evaluating the antimicrobial efficacy of tetracycline, ciprofloxacin, and amikacin, three different clinically relevant antibiotic compounds commonly used to combat AMR-related infections[9] (Supplementary Material Sec. S7.4.1), against an ampicillin-resistant strain of *E. coli* bacteria used as a demonstrative model. Briefly, all bacteriological experiments involved the generation of a gradient between antibiotic stock solutions and growth media using the fabricated μ-CGG prototype; the addition of metabolic indicator solution and *E. coli* inoculation to each discrete device output μ-drug cocktail solution collected on a 96-well plate, followed by incubation and detection. Resazurin salt (further discussed in Supplementary Material Sec. S6.1) was employed in these studies as a redox indicator of biological metabolism. Resazurin (dark blue in appearance) is readily metabolized to produce a bright pink molecule, resorufin, whereby the rate of resorufin production in solution is proportional to the

rate of respiration of viable cells. Fluorescence microscopy is a well-suited method to detect resorufin production[68], as resorufin is highly fluorescent (peak $l_{ex} = 579$ nm, $l_{em} = 584$ nm), whereas resazurin is weakly fluorescent. Resazurin-based cell viability protocols have proven simple, accurate, and reproducible methods to quantify and assess the metabolic activity of organisms, particularly bacteria[38,69,70]. In this work, normalized emission of resorufin was measured and used to produce a normalized growth (N_g) value elucidating the degree of bacterial proliferation, and thereby the antibiotic-induced bacterial growth inhibition, in each solution[71,72].

Single-antibiotic MIC testing

Experimental single-antibiotic MIC testing results are presented in Fig. 5. For each antibiotic, triplicate experiments were performed with the antibiotic solution into device inlet 1 and growth media solutions into inlets 2 and

Fig. 5 Experimental single-antibiotic minimum inhibitory concentration (MIC) testing bacteriological results, antibiotic solution input into device inlet 1, and growth media input into inlets 2 and 3 for all experiments. a Tetracycline, **b** ciprofloxacin, and **c** amikacin antibiotic MIC experiments, performed in triplicate. Top: mean normalized growth values and standard deviation error bars of fluid outputs capturing a gradient from 100% antibiotic to 100% buffer along one edge of the device, data representing the MIC value indicated by colored bars and calculated concentration. Middle: a table showing the concentrations of each of the antibiotics contained in the solution output from each device outlet. Bottom: illustration of the inputs into the microchannel network, device outlet-numbering convention and indication of the outlets containing 100% antibiotic and 100% buffer solutions

3. Mean N_g values for solutions containing μ-drug cocktails from 100% antibiotic to 100% buffer are plotted from outlets along one edge of the device, i.e., outlets 1, 3, 5, 7, 8, and 13. The MIC value of the antibiotic was determined with the first apparent stepwise reduction in mean N_g value, i.e., enhancement in growth inhibition. The diagram in Supplementary Material Fig. S11a was then used to calculate the MIC value in mg/L. All experimentally determined MIC values, as well as MIC values from the literature, are presented in Supplementary Material Fig. S12.

Tetracycline has been one of the safest and most effective antibiotics used to treat serious conditions such as syphilis, cholera, malaria, and the plague and is also useful in multi-drug treatments for AMR-related infections, such as bacterial peptic ulcers[20,73]. The tetracycline-buffer-buffer gradient (Fig. 5a) results indicated that the MIC value was represented by the μ-drug cocktail from outlet 5. It exhibited normalized growth of ~20% corresponding to a tetracycline concentration of ~0.26 mg/L, which is near the range for similar strains of *E. coli* in prior works[9,74]. The μ-drug cocktails containing higher concentrations of tetracycline than that from outlet 5 showed equivalent or lower amounts of growth, whereas those containing lower concentrations of tetracycline showed higher amounts of growth, between ~60% and 100%.

Ciprofloxacin is a commonly used antibiotic to combat UTIs, respiratory infections, and gastroenteritis and is often effective in combination with other antibiotics to treat AMR-related infections in CDS applications[16,25,30,75]. The experimental ciprofloxacin–buffer–buffer gradient (Fig. 5b) results indicated that the MIC value corresponded to the μ-drug cocktail from outlet 5. The μ-drug cocktail exhibited normalized growth of ~5%, corresponding to a ciprofloxacin concentration of ~50 μg/L, which is in agreement with the documented range for similar known multidrug AMR strains of *E. coli*[74,76]. Solutions containing higher concentrations of tetracycline showed roughly the same amount of growth, whereas those containing lower concentrations of ciprofloxacin show increased amounts of growth, ≤ ~50%.

Amikacin is a particularly effective antibiotic in combination treatments used to combat infections such as

serious UTIs, tuberculosis and bacterial meningitis, and AST evaluation of amikacin is frequently performed in clinical and drug development settings[16,76–79]. The results from the amkacin–buffer–buffer gradient (Fig. 5c) study indicated that the MIC value was represented by the μ-drug cocktail from outlet 8. This cocktail exhibited normalized growth of ~30%, corresponding to a ciprofloxacin concentration of ~11 mg/L, which agrees well with the documented range of amikacin MIC values for similar strains of *E. coli*[20,74,79]. Solutions containing higher concentrations of amikacin showed equivalent or lesser growth, whereas the solution from outlet 13 containing no antibiotics showed the highest amount of growth.

Pairwise antibiotic CDS studies

The fabricated 3D μ-CGG prototype was also proposed for use as an AST tool to perform pairwise CDS studies. Triplicate experiments were performed with two different antibiotic solutions in device inlets 1 and 3 and growth media solution in inlet 2. Mean N_g values for solutions representing the gradient between 100% of both antibiotics collected from outlets 1, 3, 5, 7, 8, and 13 are plotted. The combined effects of each antibiotic pair follow similar trends from prior AST studies with related bacterial strains[16,25,45,80,81]. The specific ampicillin-resistant *E. coli* used in this work were experimentally assessed by comparing the N_g values of each solution, as shown in pairwise antibiotic CDS results in Fig. 6.

The gradient between tetracycline and ciprofloxacin (Fig. 6a) exhibited the expected antagonism[25] in the solution from outlet 3 (~0.34 mg/L tetracycline, ~28.8 μg/L ciprofloxacin). This specific chemistry should therefore be avoided in treating an infection caused by this specific strain of bacteria. Furthermore, the gradient between amikacin and ciprofloxacin (Fig. 6b) demonstrated the expected synergism[16,45] in the solutions from outlets 5 (~7.68 mg/L amikacin, ~48.8 μg/L ciprofloxacin), and 8 (~6.08 mg/L amikacin, ~65.3 μg/L ciprofloxacin); these specific chemistries are therefore be highly recommended in treating such an infection. Moreover, the gradient between tetracycline and amikacin (Fig. 6c) revealed the expected additive effect[80,81] in all solutions from outlets 3, 5, 7, and 8; therefore, none of these solutions would serve as inherently beneficial treatments. All other solutions not explicitly mentioned demonstrated additive effects and are therefore not recommended as effective treatments.

Three-antibiotic CDS assessment

Finally, the ultimate capability for AST evaluation of more than two antimicrobial agents was demonstrated using all three antibiotic solutions. Here, every single operation of the device generated three distinct pairwise gradients between amikacin and tetracycline (outlets 1, 3, 5, 8, and 13), amikacin and ciprofloxacin (outlets 1, 2, 4, 6,

and 9), and ciprofloxacin and tetracycline (outlets 9, 10, 11, 12, and 13), in addition to the implementation of a three-antibiotic μ-drug cocktail, simultaneously.

The mean N_g data from the three-antibiotic CDS experiments (Fig. 6d) revealed the expected additive effect between amikacin and tetracycline (outlets 3 and 5), synergism between amikacin and ciprofloxacin (outlets 2, 4, and 6) and antagonism between ciprofloxacin and tetracycline (outlets 10, 11, and 12). Furthermore, an unexpected synergistic pairwise interaction was exhibited between amikacin and tetracycline from outlet 8. As a result, this specific chemistry would be recommended in treating an infection caused by the ampicillin-resistant *E. coli* strain, as demonstrated in this work. It should be noted that the metrics of three-antibiotic interactions are defined here as being relative to the interaction between any two of the antibiotics if they were to be combined in a two-antibiotic pair without the addition of the third antibiotic. As a result, the μ-drug cocktail containing a nearly equivalent proportion of all three input antibiotic compound concentrations (outlet 7) demonstrated synergism compared to the 100% solutions of amikacin and ciprofloxacin and an additive effect compared to the 100% solutions of amikacin and tetracycline, as well as ciprofloxacin and tetracycline. In this demonstration, the μ-drug cocktails from outlets 2, 4, 5, 6, 8, and 13 exhibited more effective inhibition of bacterial proliferation than those of the three-antibiotic μ-drug cocktail and would, therefore, represent more effective doses for treatment. Regardless, the three-antibiotic μ-drug cocktail is the direct result of the unique 3D fluidic routing capability demonstrated by the 3D μ-CGG microchannel network, which is otherwise impossible using planar fluidic routing processes.

Discussion

The throughput of multidrug AST applications using conventional μ-CGG devices is fundamentally limited by the inability of such systems to generate symmetric concentration gradients of more than two antimicrobial solutions at a time. In this work, we developed a 3D μ-CGG prototype employing a truly 3D microchannel network through the use of an additive manufacturing approach to accomplish fluidic routing in three dimensions to generate symmetric three-fluid concentration gradients.

Analytical modeling and theoretical simulations were used to design and optimize the microchannel network via the inclusion of embedded 3D μ-mixing structures to produce 13 distinct output μ-drug cocktail solutions for bacteriological studies. Experimental characterizations validated the generated concentrations to within 10% of the predicted values, justifying the use of the proposed 3D μ-CGG system for multidrug AST evaluations.

As a proof-of-concept, the fabricated prototype was used to evaluate the efficacy of three clinically relevant antibiotic compounds against model antibiotic-resistant
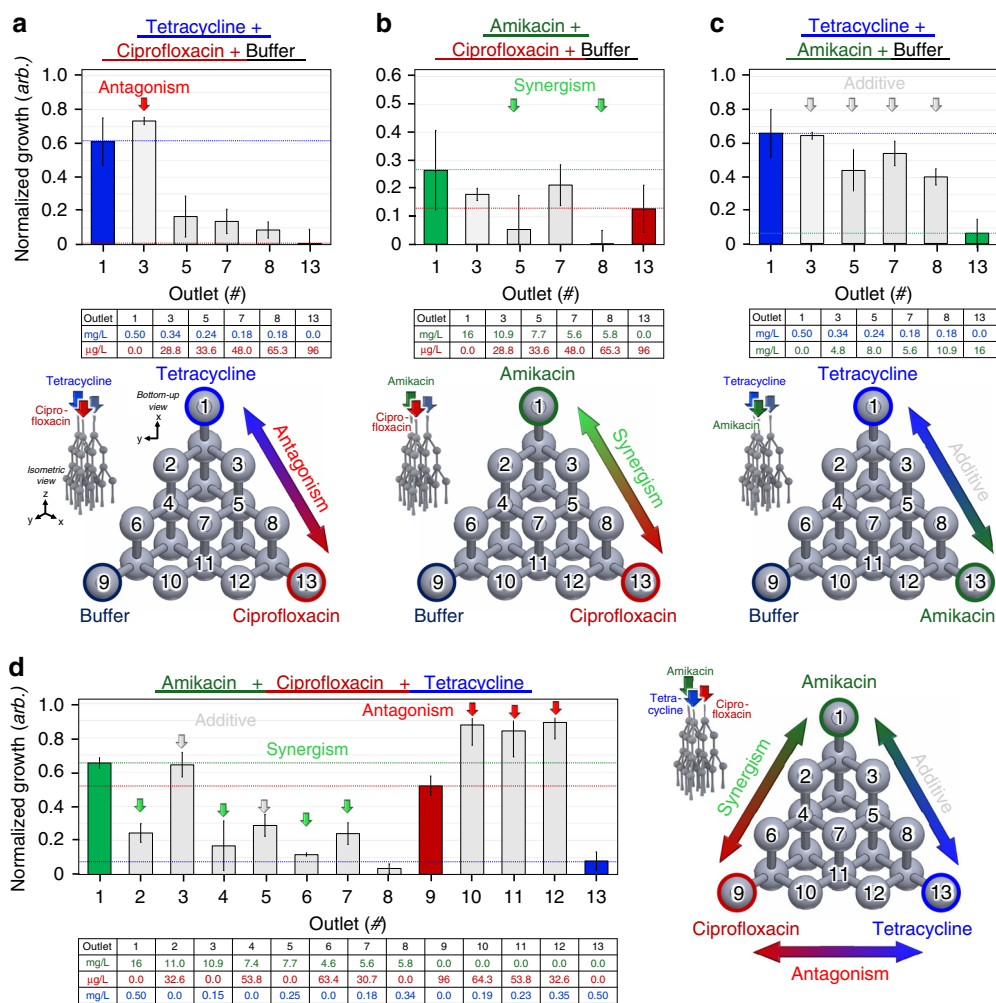
Fig. 6 Experimental combination drug screening (CDS) bacteriological results revealing inhibitory interactions between all combinations of antibiotics, and experiments were performed in triplicate. *Pairwise* interaction studies with antibiotic input into inlets 1 and 3 and growth media input into inlet 2: **a** tetracycline + ciprofloxacin, antagonism (red arrow); **b** amikacin + ciprofloxacin, synergism (green arrow); and **c** tetracycline + amikacin, additive effect (gray arrow). Top: mean normalized growth values and standard deviation error bars of fluid outputs capturing a gradient between 100% of each antibiotic; data represent the known antibiotic interaction indicated by colored arrows. Middle: a table showing the concentrations of each of the antibiotics contained in the solution output from each device outlet. Bottom: illustrations of antibiotic inputs, device outlet-numbering convention, and an indication of outlets containing 100% of each antibiotic and buffer. **d** Three-antibiotic interaction study with antibiotic input into inlets 1, 2, and 3; (left) mean normalized growth values and standard deviation error bars of all 13 fluid outputs, data representing known antibiotic interactions indicated by colored arrows; (right) illustrations of the antibiotic inputs, device outlet-numbering convention and indication of outlets containing 100% of each antibiotic

E. coli bacteria. The MIC values of the individual antibiotics were characterized and were in agreement with the documented ranges for each compound. Furthermore, the known synergistic, additive, and antagonistic effects of each combination of antibiotics were experimentally observed through individual pairwise CDS studies.

As such, the unique 3D fluidic routing capabilities enabled a three-antibiotic CDS study to simultaneously generate three distinct pairwise antibiotic concentration gradients, including one μ-drug cocktail containing all three antibiotic species, in 5 h from a single operation for

enhanced throughput over conventional multi-antimicrobial CDS approaches.

Moving forward, additive manufacturing permits straightforward and on-demand modification of 3D μ-CGG designs to produce tailored concentration gradient characteristics. Such devices can be rapidly prototyped and fabricated in clinical point-of-care settings using commercially available 3D printers to reduce the time-to-deployment and manufacturing costs. Ongoing technological advances in additive manufacturing resolution, material variety, and scalability will enable engineering of

evermore advanced 3D μ-CGG designs that can be incorporated into more complex micrototal analytical systems to significantly increase the throughput of AST to combat emerging antibiotic-resistant bacterial infections in clinical and drug development settings.

Materials and methods
Design of the 3D microchannel network
All microfluidic designs were modeled using Solidworks computer-aided design software (Dassault Systemes, Velizy-Villacoublay, France). All inlet and outlet geometries enabled device-to-world interfacing via standard 20-gauge stainless-steel catheter couples (SC20/15, Instech, PA, USA). All microchannels, bulbs, and solid bodies were saved as individual part files then arranged in a single assembly file to produce the positive-feature network (Fig. 2a) for use in all theoretical simulations. Subtraction of the model with a solid body was used to produce the final manufacturable design (Fig. 2b), saved as a single part file, exported as an.STL file and imported to 3D-printing software for manufacturing.

Prototype fabrication and postprocessing
Additive manufacturing of the prototype was accomplished using a Projet 3000UHD Multijet modeling 3D printer (3D Systems, SC, USA) (Fig. 2c). The materials employed in this work were Visijet M3 crystal polymer[82] (3D Systems) and Visijet S100 hydroxylated wax[83] (3D Systems). Both materials (Supplementary Material Sec. S2.1) were deposited simultaneously in an inkjet-like process in ~35-μm thick layers with a lateral feature resolution as low as 50 μm[84]. The support material, which was necessary to reinforce and successfully resolve overhanging geometries such as the 3D μ-mixer rifling and hollow spherical cavities, was removed from the device after 3D printing using a previously demonstrated postprocessing protocol[66,85]. Briefly, the prototype was placed inside a preheated oven at 75 °C for 15 min with the outlets facing downwards on top of paper towels to facilitate drainage of support material from the microchannels through capillary action. The device was then submerged in a beaker containing food-grade Bayes mineral oil preheated to ~60 °C for ~10 min. The heated mineral oil was flushed through each device outlet three times using a 10-mL syringe (Cole-Palmer, IL, USA) attached to a 20-Gauge Luer stub (model LS20, Instech) until all of the interior support material was removed. Finally, the process was repeated using an aqueous soap solution and potable water to remove any residual mineral oil (Fig. 2d). For further details, see Supplementary Material Sec. S2.3.

Theoretical simulations
Computation fluid dynamics (CFD) simulations were performed using COMSOL Multiphysics (Version 4.5a,

COMSOL, Inc., CA, USA) finite element analysis software to determine the theoretical performance of all 3D models. The theoretically predicted normalized concentration (N) of the species from one inlet (C_1) at each outlet for a range of input fluid flow rates was calculated as the average N value over the entire microchannel outlet face (Fig. 3). Due to the 3D symmetry of all simulated microchannel networks, and the N values for C_1 assigned to device inlet 1 were identical to the results if C_1 was assigned to inlets 2 and 3. Therefore, in this work, only C_1 assigned as the inlet 1 input was simulated. For further details, see Supplementary Material Sec. S5.

Preparation of cell solutions
Ampicillin-resistant BL21(DE3) Gram-negative *Escherichia coli* (*E. coli*) bacteria were procured from Agilent Technologies, CA, USA[86], in 2-mL cryovials as glycerol stock and stored at −80 °C. A scraping from the glycerol stock was added to 10 mL of Lysogeny Broth (LB media), a bacteria-specific nutrient-rich solution, in a 25-mL T25 flask with a breathable filter cap (#169900, ThermoFisher Scientific, MA, USA) and enriched in a bacteria incubator at 37 °C and 4% CO_2 overnight.

The following day, ~10 µL of the solution was transferred to agar media to create a solid bacteria colony plate[10], which was stored at −4 °C for use for up to 1 month. Before each day of bacteriological experiments, a fresh bacterial inoculation was created by adding a single bacterial colony harvested from the agar plate to 10 mL of LB media and incubating overnight at 37 °C. The cell density of the solution was measured the next day using a UV-VIS spectrophotometer (Vernier, OR, USA) following the OD600 method[8,87]; then, a serial dilution was performed to create an inoculation with an initial cell density of ~5×10^5 cfu/mL following cell viability[88−90] and AST[38,50,52,69,91] conventions. LB media was prepared by dissolving LB powder (LB Miller Broth, Sigma-Aldrich, MO, USA) in deionized (DI) water to make a 25 g/L solution in a 1000-mL autoclave bottle (ThermoFisher Scientific), followed by autoclave sterilization at 120 °C for 25 min. For further details, see Supplementary Material Sec. S6.2.

Preparation of reagents and antibiotic solutions
Whenever solids were added to liquids or multiple solutions were combined to create new solutions, sterile 50-mL conical polypropylene centrifuge tubes (#339652, ThermoFisher Scientific) were used, aggravated using a vortex mixer (Vortex-Genixe 2, Scientific Industries, NY, USA) for ~30 s to ensure a homogeneous solution, and then wrapped in aluminum foil and stored at −4 °C for up to 1 week of use. Rhodamine fluorescent dye solution was created by adding 50 drops of 0.04% fluorescent red dye Rhodamine B solution (OnlineScienceMall) to 50 mL of DI

water. Resazurin metabolic indicator solution was prepared to a concentration of ~4.4 mM by adding ~5 mg of resazurin salt powder (Sigma-Aldrich) to 50 mL of sterile LB media. Antibiotic solutions were prepared by combining the required mass of antibiotic powder (each acquired from Sigma-Aldrich) to 500 mL of sterile LB media to create the desired antibiotic stock solution concentration, roughly twice the approximate average of published MIC values for a specific antibiotic against *E. coli*. For all concentrations of antibiotic stock solutions used throughout this work, see Supplementary Material Fig. S12.

Device operation and collection of output gradients

Discrete fluidic outputs from the fabricated 3D μ-CGG prototype were collected using the experimental setup conceptually illustrated in Fig. 2e. Briefly, for each experiment, fluids from three independent fluidic reservoirs attached to a MAESFLO microfluidic control platform (Fluigent, Paris, France) were pressure-driven through the three device inlets at a steady volumetric flow rate of 1000 μL/min for one minute. The device output solutions, each contained in discrete segments of Tygon tubing (#06420-03, Cole-Palmer, IL, USA) cut to length to isolate the desired volume, were routed to discrete wells on a standard microwell plate (ThermoFisher Scientific). See Supplementary Material Sec. S7.1 for further details.

Experimental fluid flow characterization

The 3D μ-CGG device was used to generate gradients between one rhodamine fluorescent dye solution and two DI water inputs, and 90 μL of output solution was collected on a 96-well plate. Briefly, using the fluorescence imaging setup (Fig. 2f), the normalized concentration of rhodamine in each solution, averaged over three experiments, was determined by imaging each solution under UV light excitation inside a custom-built light isolation box with a red bandpass optical filter (610-700 nm, #W6308, Omega Optical, VT, USA) and DSLR camera (Canon EOS 1000D, Canon, Tokyo, Japan), and the excitation and emission peaks of rhodamine were set as 540 nm and 625 nm, respectively[92]. Rhodamine fluorescence emission in each solution was quantified using the image analysis protocol detailed in Supplementary Material Sec. S7.3.

Bacteriological AST experiments

For each experiment, the 3D μ-CGG device was used to generate gradients between antibiotic and buffer solutions. The output (30 μL) μ-drug cocktail solutions were collected on a 96-well plate, then 30 μL of each resazurin metabolic indicator solution and *E. coli* inoculation were pipetted into each well. A 0% antibiotic (fully uninhibited proliferation) control consisting of 30 μL each of bacterial inoculation, resazurin solution, and LB media was pipetted into one well, and the no-proliferation control,

consisting of 30 μL of resazurin solution and 60 μL of LB media, was pipetted into another well. For further details, see Supplementary Material S7.4. Each plate was first incubated at 37 °C (Fig. 2f) until a visible gradient between blue and pink from the 0% antibiotic control across the device outputs was observed for an average of ~5 h. The normalized bacterial proliferation in each solution, averaged over three experiments, was determined by imaging each solution under excitation from green LED light[69] using a 585-nm optical filter (#W6308, Omega Optical)[93]. The fluorescence emission of resorufin in each solution was quantified following the image analysis protocol detailed in the Supplementary Material Sec. S7.4.

Author details
[1]Department of Mechanical Engineering, University of California, Berkeley, CA 94720, USA. [2]Berkeley Sensor and Actuator Center, Berkeley, CA 94720, USA. [3]Department of Bioengineering, University of California, Berkeley, CA 94720, USA. [4]Department of Materials Science and Engineering, University of California, Berkeley, CA 94720, USA

Author contributions
E.S. and J.C. conceived and modeled the designs; E.S., B.Y., and J.C. designed the experiments; E.S., B.Y., J.C., R.V., Y.L., A.L., E.J., T.W., C.M., S.L., and A.C. performed the experiments; E.S., R.V., Y.L., E.J., T.W., R.J., and Y.A. analyzed the data; E.S. wrote the paper; and L.L. supervised the project and edited the paper.

Conflict of interest
The authors declare that they have no conflicts of interest.

References
1. Avesar, J. et al. Rapid phenotypic antimicrobial susceptibility testing using nanoliter arrays. *Proc. Natl Acad. Sci. USA* **114**, E5787 LP–E5785785795 (2017).
2. ONeill, J. Antimicrobial resistance: tackling a crisis for the health and wealth of nations. *Rev. Antimicrob. Resist.* **2019**, 1–18 (2014).
3. Conly, J. & Johnston, B. Where are all the new antibiotics? The new antibiotic paradox. *Can. J. Infect. Dis. Med. Microbiol.* **16**, 159–160 (2005).
4. CDC. Antibiotic resistance threats in the United States. *U.S. Dep. Heal. Hum. Serv.* **114**. https://doi.org/10.15620/cdc:82532 (Atlanta, GA: U.S. Department of Health and Human Services, CDC, 2019).
5. Cars, O., Hedin, A. & Heddini, A. The global need for effective antibiotics, moving towards concerted action. *Drug Resist. Updat.* **14**, 68–69 (2011).
6. Wilkerson, C., Samadpour, M., Van Kirk, N. & Roberts, M. C. Antibiotic resistance and distribution of tetracycline resistance genes in *Escherichia coli* O157H7 isolates from humans and bovines. *Antimicrob. Agents Chemother.* **48**, 1066–1067 (2004).
7. CLSI. Performance standards for antimicrobial susceptibility testing performance standards for antimicrobial suscepti-bility testing suggested citation. *CLSI Doc.* **M02-A11**, 100–125 (2018).

8. Wiegand, I., Hilpert, K. & Hancock, R. E. W. Agar and broth dilution methods to determine the minimal inhibitory concentration (MIC) of antimicrobial substances. *Nat. Protoc.* **3**, 163–175 (2008).

9. Andrews, J. M. Determination of minimum inhibitory concentrations. *J. Antimicrob. Chemother.* **48**, 5–16 (2001).

10. Saint Ruf, C. et al. Antibiotic susceptibility testing of the gram negative bacteria based on flow cytometry. *Front. Microbiol.* **7**, 1–13 (2016).

11. European Society of Clinical Microbiology and Infectious Diseases. Determination of minimum inhibitory concentrations of antibacterial agents by broth dilution. *Clin. Microbiol. Infect.* **9**, 1–7 (2003).

12. Hudzicki, J. Kirby-Bauer disk diffusion susceptibility test protocol. *Am. Soc. Microbiol.* 1–13 (2012).

13. Dallas, S. D. et al. Development of doxycycline MIC and disk diffusion interpretive breakpoints and revision of tetracycline breakpoints for Streptococcus pneumoniae. *J. Clin. Microbiol.* **51**, 1798–1802 (2013).

14. Liu, X. et al. High-throughput screening of antibiotic-resistant bacteria in picodroplets. *Lab Chip* **16**, 1636–1643 (2016).

15. Shembekar, N., Chaipan, C., Utharala, R. & Merten, C. A. Droplet-based microfluidics in drug discovery, transcriptomics and high-throughput molecular genetics. *Lab Chip* **16**, 1314–1331 (2016).

16. Al-Muharrmi, Z., Rafay, A., Balkhair, A. & Jabri, A. A. Antibiotic combination as empirical therapy for extended spectrum Beta-lactamase. *Oman Med. J.* **23**, 78–81 (2008).

17. Tamma, P. D., Cosgrove, S. E. & Maragakis, L. L. Combination therapy for treatment of infections with Gram-negative bacteria. *Clin. Microbiol. Rev.* **25**, 450–470 (2012).

18. Zimmer, A., Katzir, I., Dekel, E., Mayo, A. E. & Alon, U. Prediction of multidimensional drug dose responses based on measurements of drug pairs. *Proc. Natl Acad. Sci. USA* **113**, 10442–10447 (2016).

19. Jain, S. N. & Sampath, A. Antibiotic synergy test: checkerboard method on multidrug resistant pseudomonas aeruginosa. *Res. J. Pharm.* **2**, 2011 (2011).

20. Yeh, P., Tschumi, A. I. & Kishony, R. Functional classification of drugs by properties of their pairwise interactions. *Nat. Genet.* **38**, 489–494 (2006).

21. Dafale, N. A., Semwal, U. P., Rajput, R. K. & Singh, G. N. Selection of appropriate analytical tools to determine the potency and bioactivity of antibiotics and antibiotic resistance. *J. Pharm. Anal.* **6**, 207–213 (2016).

22. Lu, Y. et al. Single cell antimicrobial susceptibility testing by confined microchannels and electrokinetic loading. *Anal. Chem.* **85**, 3971–3976 (2013).

23. Puttaswamy, S., Gupta, S. K., Regunath, H., Smith, L. P. & Sengupta, S. A comprehensive review of present and future antibiotic susceptibility testing systems. *Arch. Clin. Microbiol.* **09**, 1–9 (2018).

24. Campbell, J. et al. Microfluidic advances in phenotypic antibiotic susceptibility testing. *Biomed. microdevices* **18**, 103 (2016).

25. Oluyemi Omoya, F. & Oluyemi Ajayi, K. Synergistic effect of combined antibiotics against some selected multidrug resistant human pathogenic bacteria isolated from poultry droppings in Akure, Nigeria. *Adv. Microbiol.* **06**, 1075–1090 (2016).

26. Bollenbach, T. Antimicrobial interactions: mechanisms and implications for drug discovery and resistance evolution. *Curr. Opin. Microbiol.* **27**, 1–9 (2015).

27. Kidsley, A. K. et al. Antimicrobial susceptibility of *Escherichia coli* and salmonella spp. isolates from healthy pigs in Australia. *Front. Microbiol.* **9**, 1–11 (2018).

28. Bollenbach, T., Quan, S., Chait, R. & Kishony, R. Nonoptimal microbial response to antibiotics underlies suppressive drug interactions. *Cell* **139**, 707–718 (2009).

29. Cira, N. J., Ho, J. Y., Dueck, M. E. & Weibel, D. B. A self-loading microfluidic device for determining the minimum inhibitory concentration of antibiotics. *Lab Chip* **12**, 1052–1059 (2012).

30. Watkinson, A. J., Micalizzi, G. R., Bates, J. R. & Costanzo, S. D. Novel method for rapid assessment of antibiotic resistance in *Escherichia coli* isolates from environmental waters by use of a modified chromogenic agar. *Appl. Environ. Microbiol.* **73**, 2224–2229 (2007).

31. Khan, I. U., Serra, C. A., Anton, N. & Vandamme, T. Microfluidics: a focus on improved cancer targeted drug delivery systems. *J. Control. Release* **172**, 1065–1074 (2013).

32. Nguyen, N.-T., Shaegh, S. A. M., Kashaninejad, N. & Phan, D.-T. Design, fabrication and characterization of drug delivery systems based on lab-on-a-chip technology. *Adv. Drug Deliv. Rev.* **65**, 1403–1419 (2013).

33. An, D., Kim, K. & Kim, J. Microfluidic system based high throughput drug screening system for curcumin/TRAIL combinational chemotherapy in human prostate cancer PC3 cells. *Biomol. Ther.* **22**, 355–362 (2014).

34. Cui, P. & Wang, S. Application of microfluidic chip technology in pharmaceutical analysis: a review. *J. Pharm. Anal.* **9**, 238–247 (2019).

35. Tang, M. et al. A linear concentration gradient generator based on multi-layered centrifugal microfluidics and its application in antimicrobial susceptibility testing. *Lab Chip* **18**, 1452–1460 (2018).

36. Damiati, S., Kompella, U. B., Damiati, S. A. & Kodzius, R. Microfluidic devices for drug delivery systems and drug screening. *Genes* **9**, https://doi.org/10.3390/genes9020103 (2018).

37. Monie, D. D. & Bhatia, S. K. *Bioprinting of Dynamic Human Organs-on-Chips: Enabling Technologies for Rapid Drug Development and Personalized Medicine.* In Turksen K (ed) Bioprinting in Regenerative Medicine, 123–137 (Springer International Publishing, Cham, Switzerland, 2015).

38. Boedicker, J. Q., Li, L., Kline, T. R. & Ismagilov, R. F. Detecting bacteria and determining their susceptibility to antibiotics by stochastic confinement in nanoliter droplets using plug-based microfluidics. *Lab Chip* **8**, 1265–1272 (2008).

39. Kim, S., Cestellos Blanco, S., Inoue, K. & Zare, R. Miniaturized antimicrobial susceptibility test by combining concentration gradient generation and rapid cell culturing. *Antibiotics* **4**, 455–466 (2015).

40. Worthington, R. J. & Melander, C. Combination approaches to combat multi-drug resistant bacteria, the problem of multi drug-resistant bacteria. *Trends Biotechnol.* **31**, 177–184 (2012).

41. Young, E. W. K. & Beebe, D. J. Fundamentals of microfluidic cell culture in controlled microenvironments. *Chem. Soc. Rev.* **39**, 1036–1048 (2010).

42. Mach, K. E. et al. A biosensor platform for rapid antimicrobial susceptibility testing directly from clinical samples. *J. Urol.* **185**, 148–153 (2011).

43. Bates, J. et al. Point of care testing for urinary tract infection in primary care (POETIC): protocol for a randomised controlled trial of the clinical and cost effectiveness of FLEXICULT informed management of uncomplicated UTI in primary care. *BMC Fam. Pract.* **15**, 1–9 (2014).

44. Zhu, H., Yaglidere, O., Su, T.-W., Tseng, D. & Ozcan, A. Cost-effective and compact wide-field fluorescent imaging on a cell-phone. *Lab Chip* **11**, 315–322 (2011).

45. Matsumoto, Y. et al. A microfluidic channel method for rapid drug-susceptibility testing of Pseudomonas aeruginosa. *PLoS ONE* **11**, 1–17 (2016).

46. Kim, C. et al. A serial dilution microfluidic device using a ladder network generating logarithmic or linear concentrations. *Lab Chip* **8**, 473–479 (2008).

47. Hu, C., Liu, J., Chen, H. & Nie, F. Microfluidic platforms for gradient generation and its applications. *Biochem. Anal. Biochem.* **6**, 2161–1009 (2017).

48. Dertinger, S. K. W., Chiu, D. T., Jeon, N. L. & Al., E. Generation of gradients having complex shapes using microfluidic networks. *Anal. Chem.* **73**, 1240–1246 (2001).

49. Toh, A. G., Wang, Z. P., Yang, C. & Nguyen, N. T. Engineering microfluidic concentration gradient generators for biological applications. *Microfluid. Nanofluidics* **16**, 1–18 (2014).

50. Malmberg, C. et al. A novel microfluidic assay for rapid phenotypic antibiotic susceptibility testing of bacteria detected in clinical blood cultures. *PLoS ONE* **11**, 1–15 (2016).

51. Eduati, F. et al. A microfluidics platform for combinatorial drug screening on cancer biopsies. *Nat. Commun.* **9**, 2434 (2018).

52. Chen, J., Picard, R. A., Wang, D. & Nugen, S. R. Lyophilized engineered phages for *Escherichia coli* detection in food matrices. *ACS Sens.* **2**, 1573–1577 (2017).

53. Hong, B. et al. A concentration gradient generator on a paper-based microfluidic chip coupled with cell culture microarray for high-throughput drug screening. *Biomed. Microdevices* **18**, 1–8 (2016).

54. Abdallah, B. G., Roy Chowdhury, S., Fromme, R., Fromme, P. & Ros, A. Protein crystallization in an actuated microfluidic nanowell device. *Cryst. Growth Des.* **16**, 2074–2082 (2016).

55. Flentie, K. et al. Microplate-based surface area assay for rapid phenotypic antibiotic susceptibility testing. *Sci. Rep.* **9**, 1–9 (2019).

56. Temiz, Y., Lovchik, R. D., Kaigala, G. V. & Delamarche, E. Lab-on-a-chip devices: How to close and plug the lab? *Microelectron. Eng.* **132**, 156–175 (2015).

57. Ha, J. H., Kim, T. H., Lee, J. M., Ahrberg, C. D. & Chung, B. G. Analysis of 3D multi-layer microfluidic gradient generator. *Electrophoresis* **38**, 270–277 (2017).

58. Zheng, Y., Wu, J., Shao, J., Jin, Q. & Zhao, J. Development of a novel perfusion microfluidic cell culture device for cell-based assays. In *2009 4th IEEE International Conference on Nano/Micro Engineered and Molecular Systems*. 257–260. https://doi.org/10.1109/NEMS.2009.5068572 (IEEE, 2009).

59. Sochol, R. D. et al. 3D printed microfluidics and microelectronics. *Microelectron. Eng.* **189**, 52–68 (2017).

60. Chen, X. et al. 3D printed microfluidic chip for multiple anticancer drug combinations. *Sens. Actuators, B: Chem.* **276**, 507–516 (2018).

61. He, Y., Wu, Y., Fu, J. Z., Gao, Q. & Qiu, J. J. Developments of 3D printing microfluidics and applications in chemistry and biology: a review. *Electroanalysis* **28**, 1658–1678 (2016).

62. Shallan, A. I., Smejkal, P., Corban, M., Guijt, R. M. & Breadmore, M. C. Cost-effective three-dimensional printing of visibly transparent microchips within minutes. *Anal. Chem.* **86**, 3124–3130 (2014).

63. Dai, J., Hamon, M. & Jambovane, S. Microfluidics for antibiotic susceptibility and toxicity testing. *Bioengineering* **3**, 25 (2016).

64. Oh, K. W., Lee, K., Ahn, B. & Furlani, E. P. Design of pressure-driven microfluidic networks using electric circuit analogy. *Lab Chip* **12**, 515–545 (2012).

65. Jeon, N. L. et al. Generation of solution and surface gradients using microfluidic systems. *Langmuir* **16**, 8311–8316 (2000).

66. Sweet, E. C. et al. 3D printed chaotic mixer for low Reynolds number microfluidics. In *2019 20th International Conference on Solid-State Sensors, Actuators and Microsystems & Eurosensors XXXIII (TRANSDUCERS & EUROSENSORS XXXIII)* 2258–2261 (IEEE, 2019).

67. Locascio, L. E. Microfluidic mixing. *Anal. Bioanal. Chem.* **379**, 325–327 (2004).

68. Promega Corporation. Technical Bulletin: CellTiter-Blue® Cell Viability Assay (Promega Corporation, Madison, WI, 2016).

69. Churski, K. et al. Rapid screening of antibiotic toxicity in an automated microdroplet system. *Lab Chip* **12**, 1629–1637 (2012).

70. In Vitro Toxicology Assay Kit, Resazurin based; MSDS No. TOX8 [Online]; May 4th, 2019. https://www.sigmaaldrich.com/catalog/product/sigma/tox8?lang=en®ion=US (Sigma-Aldrich Inc., St. Louis, MO, 2019).

71. Udekwu, K. I., Parrish, N., Ankomah, P., Baquero, F. & Levin, B. R. Functional relationship between bacterial cell density and the efficacy of antibiotics. *J. Antimicrob. Chemother.* **63**, 745–757 (2009).

72. Sarker, S. D., Nahar, L. & Kumarasamy, Y. Microtitre plate based antibacterial assay incorporating resazurin as an indicator of cell growth and its application in the in vitro antibacterial screening of phytochemicals. *Methods* **42**, 321–324 (2007).

73. Duployez, C., Robert, J. & Vachee, A. Trimethoprim susceptibility in *E. coli* community acquired urinary tract infections in France. *Med. et. Maladies Infect.* **48**, 410–413 (2018).

74. Sabir, S. et al. Isolation and antibiotic susceptibility of *E. coli* from urinary tract infections in a tertiary care hospital. *Pak. J. Med. Sci.* **30**, 389–392 (2014).

75. Eliopoulos, G. M. & Eliopoulos, C. T. Ciprofloxacin in combination with other antimicrobials. *Am. J. Med.* **87**, S17–S22 (1989).

76. Miranda, E. J. P. D. et al. Susceptibility to antibiotics in urinary tract infections in a secondary care setting in Sao Paulo, Brazil, From Urine Cultures. *Rev. do Inst. de. Med. Trop. de. Sao Paulo* **56**, 313–324 (2014).

77. Promega Corporation. Product Monograph: Amikacin Sulfate Injection USP. (Omega Laboratories Limited, Boucherville, QC, Canada, 2019).

78. Dionex. Analysis of the aminoglycoside antibiotics kanamycin and amikacin matches USP requirements. application note 267. *Appl. Note* **267**, 1–6 (2011).

79. Sutherland, C. A., Verastegui, J. E. & Nicolau, D. P. In vitro potency of amikacin and comparators against *E. coli*, *K. pneumoniae* and *P. aeruginosa* respiratory and blood isolates. *Ann. Clin. Microbiol. Antimicrob.* **15**, 1–7 (2016).

80. Zhao, J., Liu, W., Lv, G., Shen, Y. & Wu, S. Protothecosis successfully treated with amikacin combined with tetracyclines. Fallbericht. Protothecose erfolgreich mit amikacin plus tetracyclinen behandelt. *Mycoses* **47**, 156–158 (2004).

81. Kuti, J. L. et al. Defining the potency of amikacin against *Escherichia coli*, *Klebsiella pneumoniae*, *Pseudomonas aeruginosa*, and *Acinetobacter baumannii*. *Infect. Drug Resist.* **11**, 783–790 (2018).

82. 3D Systems. VisiJet M3 crystal. *Mater. Data Sheet* **1**, 1–7 (2016).

83. 3D Systems. Visijet S100. *Mater. Data Sheet* **1910**, 8–10 (2012).

84. Glick, C. C. et al. Rapid assembly of multilayer microfluidic structures via 3D-printed transfer molding and bonding. *Microsyst. Nanoeng.* **2**, 16063 (2016).

85. Sochol, R. D. et al. 3D printed microfluidic circuitry via multijet-based additive manufacturing. *Lab Chip* **16**, 668–678 (2016).

86. BL21(DE3) Competent cells. Catalog #200131; Instruction Manual [Online]. https://www.agilent.com/cs/library/usermanuals/public/200133.pdf (Agilent Technologies, Inc.: Santa Clara, CA, 2015).

87. Ewell, M. D. Counting Bacteria. *Science* **ns-15**, 362–362 (2006).

88. Lee, W., Kwon, D., Choi, W., Jung, G. Y. & Jeon, S. 3D printed microfluidic device for the detection of pathogenic bacteria using size based separation in helical channel with trapezoid cross section. *Sci. Rep.* **5**, 7717 (2015).

89. Simoes, J. & Dong, T. Continuous and real-time detection of drinking water pathogens with a low cost fluorescent optofluidic sensor. *Sensors* **18**, https://doi.org/10.3390/s18072210 (2018).

90. Yang, Y., Kim, S. & Chae, J. Separating and detecting escherichia coli in a microfluidic channel for urinary tract infection applications. *J. Microelectromech. Syst.* **20**, 819–827 (2011).

91. Yao, P., Wang, R., Xi, X., Li, Y. & Tung, S. et al. 3D-printed pneumatic microfluidic mixer for colorimetric detection of Listeriamonocytogenes. *Transactions of the ASABE* **62**(3), 841–850 (2019).

92. National Center for Biotechnology Information. PubChem Compound Summary for CID 44134928, Rhodamine B isothiocyanate. Retrieved 31 Aug 2020 from https://pubchem.ncbi.nlm.nih.gov/compound/Rhodamine-B-isothiocyanate (2020).

93. Omega Optical. Material Specifications Sheet for 585BP90 RapidBand. Retrieved 31 Aug 2020 from https://www.omegafilters.com/product/2737 (2027).